Journal of Materials Chemistry A

Accepted Manuscript

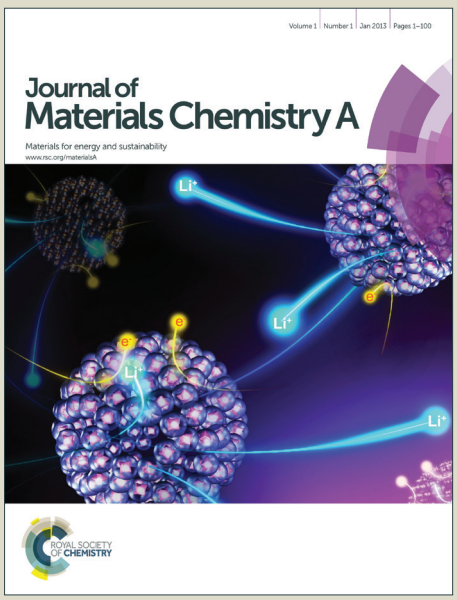

ROYAL SOCIETY OF CHEMISTRY

www.rsc.org/materialsA

Journal Name

ARTICLE

Synthesis of tri-level hierarchical SAPO-34 zeolite with intracrystalline micro-meso-macroporosity showing superior MTO performance

Received 00th January 20xx,
Accepted 00th January 20xx

DOI: 10.1039/x0xx00000x

www.rsc.org/

Qiming Sun,[a‡] Ning Wang,[a‡] Guanqi Guo,[a] Xiaoxin Chen,[a] and Jihong Yu*[a]

Hierarchically porous zeolites with different level of porosity have emerged as an important class of materials because of their enhanced mass transport and improved catalytic performance. Silicoaluminophosphate zeolite SAPO-34 is one of the best catalysts for methanol-to-olefin (MTO) conversion, but suffers from rapid deactivation due to the narrow 8-ring pore openings. To overcome the inherent diffusion bottleneck and improve the MTO performance, in this work, tri-level hierarchically porous SAPO-34 zeolite with intracrystalline micro-meso-macroporosity has been first synthesized by an Al-rich method coupled with the use of polyethylene glycol 2000 polymer under hydrothermal conditions. The as-synthesized hierarchically porous SAPO-34 catalysts exhibit superior catalytic performance in MTO reaction with about six-times prolonged catalytic lifetime and nearly 5% improvement of selectivity for ethylene and propylene than the conventional microporous SAPO-34.

1 Introduction

Zeolites with pore diameter typically less than 2 nm belong to a class of microporous crystalline materials, which are found wide application in chemical industry as the most important solid catalysts.[1-5] To overcome the pore size limitation of zeolites, hierarchically porous zeolites comprising mesopore (2~50 nm) and/or macropore (>50 nm) have attracted growing interest.[6-9] Hierarchically porous zeolites can greatly enhance the mass transport, which is particularly important for the diffusion of large molecules in various catalytic reactions. Meanwhile, hierarchically porous zeolites can also reduce the rate of forming coke deposition and increase the catalyst lifetime due to the easier mass transport over the large pore volume of meso and/or macroporous systems compared to the purely microporous system. [10-12] Up to now, various strategies have been developed for the preparation of hierarchically micro-mesoporous and micro-macroporous aluminosilicate zeolites, such as soft template route,[13-16] hard template route,[17, 18] and post-treatment route.[19, 20] The synthesis of tri-level hierarchical industrially important zeolites with superior catalytic performance is of great challenge. So far, several tri-level micro-meso-macroporous structures based on silicate zeolites have been reported. [21-24]

Silicoaluminophosphate zeolite SAPO-34 with **CHA** framework structure has attracted widespread attention because of its extraordinary activity for methanol-to-olefin (MTO) conversion. [25-31] However, the narrow 8-ring pore openings of SAPO-34 cause problem of rapid deactivation due to the mass transport resistance, leading to a large amount of organic species accommodating in the large cavities in the methanol process.[27] Previous studies have demonstrated that introducing mesopores or macropores into the microporous SAPO-34 zeolite crystals can greatly enhance the transfer of the reaction products, decrease the formation of coke, and thus prolong the catalyst lifetime.[32-35] Recently, several bi-level hierarchically porous SAPO-34 zeolites with micro-meso/macropore stucture have been synthesized, showing remarkably enhanced MTO performance. [32-34, 36, 37] However, up to now, the synthesis of tri-level hierarchically porous SAPO-34 zeolites has seen no success.

It is well known that the incorporation of silicon atoms into the $AlPO_4$-34 framework has two different substitution mechanisms. One is the SM2 mechanism that one silicon replaces one phosphorus, and another is the SM3 mechanism that two silicon atoms replace the neighboring aluminum and phosphorus.[38, 39] According to such substitution mechanisms, the Al content should be less than the total contents of Si and P. In contrast, if the Al content is greater than the total of Si and P contents in the framework, it may produce more terminal groups or defects, leading to the formation of hierarchical pores. On the other hand, various polymers have proven to be excellent mesoporous templetes by forming polymer network inside zeolite matrix.[16, 37, 40] Inspired by this design concept, in this work, the tri-level hierarchically porous SAPO-34 zeolite with intracrystalline micro-meso-macropore structure has been successfully synthesized using an Al-rich

[a] State Key Laboratory of Inorganic Synthesis and Preparative Chemistry, College of Chemistry, Jilin University, Changchun 130012, P. R. China
‡ These authors contributed equally.
Electronic Supplementary Information (ESI) available: [TG curves and the detailed MTO results over SAPO-34 catalysts, etc. are provided in the supporting information.]. See DOI: 10.1039/x0xx00000x

method coupled with the use of polyethylene glycol 2000 (PEG 2000) polymer under hydrothermal conditions for the first time. Importantly, the hierarchically porous SAPO-34 catalysts exhibit superior performance in MTO reaction with about six-times prolonged catalytic lifetime and nearly 5% improvement of selectivity for ethylene and propylene compared to the conventional microporous SAPO-34 catalyst.

2 Experiment section

2.1 Synthesis.

2.1.1 Chemical and materials: Phosphoric acid (85 wt%, Beijing Chemical Works), pseudoboehmite (Al_2O_3, 62.5 wt%, Vista), triethylamine (TEA, 99%, Fuyu company), fumed silica (Changling Refining Company), Polyethylene glycol 2000 (PEG 2000, Guangfu Reagent Company).

2.1.2 Preparation of hierarchically porous SAPO-34 catalysts (S_{H1}, S_{H2}, S_{H3}, and S_{H4}) The hierarchically porous SAPO-34 catalysts were synthesized from the Al-rich gels coupled with the use of PEG 2000 polymer with the optimized molar compositions of $2.0Al_2O_3$: $1.0P_2O_5$: 4.7TEA: $0.4SiO_2$: $70H_2O$: *x* PEG 2000 (*x* =0, 0.02 and 0.04) under hydrothermal conditions at 200 ˚C for 24h, and the resulting products were named as S_{H1}, S_{H2} and S_{H3}, respectively. As comparison, the hierarchically porous SAPO-34 catalyst S_{H4} with normal Al content using PEG 2000 polymer was synthesized under the same condition with the molar composition of $1.0Al_2O_3$: $1.0P_2O_5$: 4.7TEA: $0.4SiO_2$: $70H_2O$: 0.04 PEG 2000.

Typically, the mixture was prepared by first mixing the deionized water with phosphoric acid together with pseudoboehmite, followed by a continuous stirring for 2 h. Then triethylamine was added into the above mixture. After a continuous stirring for 1 h, fumed silica was added into the resultant solution slowly, and then stirred for 2 h continuously. Finally, the PEG 2000 was added into the mixture. The reaction mixture was further stirred for 2 h and was then transferred into a 100 mL Teflon-lined stainless steel autoclave. The crystallization was conducted in a conventional oven at 200 °C for 24 h under static conditions. The as-synthesized solid products were centrifuged, washed with water and ethanol for several times, and then dried at 80°C in the oven overnight, followed by calcination at 600 °C for 8 h.

2.1.3 Preparation of conventional SAPO-34 catalyst (S_M). The conventional microporous SAPO-34 catalysts (S_M) was synthesized from the starting gel with molar composition of $1.0Al_2O_3$: $1.0P_2O_5$: 4.7TEA: $0.4SiO_2$: $70H_2O$ under hydrothermal conditions at 200 °C. The synthesis procedure was the same as that of the hierarchically porous SAPO-34 catalysts.

2.2 Characterizations. The crystallinity and phase purity of the samples were characterized by powder X-ray diffraction on a Rigaku D-Max 2550 diffractometer using Cu Kα radiation (λ = 1.5418 Å). The crystal size and morphology were measured by a scanning electron microscopy (SEM) using a JSM-6510 (JEOL) electron microscope. Transmission electron microscopy (TEM) images were recorded with a Tecnai F20 electron microscope. Nitrogen adsorption/desorption measurements were carried out on a Micromeritics 2020 analyzer at 77.35 K after the samples were degassed at 350 °C under vacuum. Thermogravimetric (TG) analysis was performed on a Perkin-Elmer TGA7 unit in air at a heating rate of 10 K min^{-1} from room temperature to 800 °C. Chemical compositions were determined with inductively coupled plasma (ICP) analyses carried out on a Perkin-Elmer Optima 3300 DV ICP instrument. The temperature-programmed desorption of ammonia (NH_3-TPD) experiments were performed using a Micromeritics AutoChem II 2920 automated chemisorption analysis unit with a thermal conductivity detector (TCD) under helium flow. All NMR experiments were performed on Bruker AVANCE III 400 WB spectrometer. The resonance frequencies in this field strength were 161.9, 104.2, 79.5 and 400.1 MHz for ^{31}P, ^{27}Al, ^{29}Si and ^{1}H respectively. Chemical shifts were referenced to 1.0 M $Al(NO_3)_3$ for ^{27}Al, 85% H_3PO_4 for ^{31}P, and 2,2-dimethyl-2-ilapentane-5-sulfonate sodium salt (DSS) for ^{29}Si and ^{1}H. The spinning rates of the samples at the magic angle were 4, 10, 6 and 8 kHz for ^{29}Si, ^{27}Al, ^{31}P, and ^{1}H, respectively.

2.3 Catalytic test and carbon deposits analysis. Methanol conversion was performed in a quartz tubular fixed-bed reactor at atmospheric pressure. The catalyst (300 mg, 40-60 mesh) loaded in the quartz reactor with the 6 mm inner dimension was activated at 773 K in a N_2 flow of 30 mL min^{-1} for 1 h before starting each reaction run and then the temperature was adjusted to reaction temperature of 723 K. The methanol was fed by passing the carrier gas (15 mL min^{-1}) through a saturator containing methanol at 49°C, which gave a WHSV of 4.0 h^{-1}. The reaction products were analyzed using an on-line gas chromatograph (Agilent GC 7890A), equipped with a flame ionization detector (FID) and Plot-Q column (Agilent J&W GC Columns, HP-PLOT/Q 19091-Q04, 30m×320μm×20μm). The conversion and selectivity were calculated on CH_2 basis and dimethyl ether (DME) was considered as reactant in the calculation.

The amount of generated coke in SAPO-34 catalysts after the MTO reactions at 40% methanol conversion was determined by thermal analysis (TG) on a Perkin-Elmer TGA7 at a heating rate of 10 °C min^{-1} from room temperature to 800 °C under air flow.

3 Results and discussion

The hierarchically porous SAPO-34 catalysts (S_{H1}, S_{H2} and S_{H3}) were synthesized from an Al-rich gel using PEG 2000 and triethylamine (TEA) as the mesopore and micropore templetes, respectively, with optimized molar compositions of $2.0Al_2O_3$: $1.0P_2O_5$: 4.7TEA: $0.4SiO_2$: $70H_2O$: *x* PEG 2000 (*x* = 0, 0.02 and 0.04) under hydrothermal conditions at 200˚C for 24h. The hierarchically porous SAPO-34 catalyst S_{H4} was synthesized with a normal Al content gel using PEG 2000 and triethylamine (TEA) as the mesopore and micropore templetes. For comparative purpose, the conventional microporous SAPO-34 (S_M) was synthesized in the gel with molar composition of $1.0Al_2O_3$: $1.0P_2O_5$: 4.7TEA: $0.4SiO_2$: $70H_2O$ under the same synthesis condition.

The XRD patterns of all of the samples show typical diffraction peaks of the **CHA** structure with high crystallinity (Figure 1a), proving the phase purity of as-synthesized SAPO-34. Figure 2 shows the SEM images of the hierarchically porous

SAPO-34 crystals as compared with the conventional one. All of the samples exhibit characteristic cubic-like morphology with particle sizes ranging from 5 to 10 μm. In contrast to the conventional microporous SAPO-34 crystals with smooth crystal surface, the hierarchically porous SAPO-34 crystals show the rough surface. The hierarchically porous SAPO-34 crystals synthesized by Al-rich method show center-hollowed morphology with many macroholes on their surfaces. A butterfly-like boundary can also be observed, indicating the intergrowth structure of the hierarchically porous SAPO-34 crystals.[34] TEM images clearly reveal the existence of macropores extending along the entire crystals with the pore size of about 50-100 nm in the hierarchical SAPO-34 crystals synthesized by Al-rich method (Figure 3). Some mesopores can also be observed in S_{H2}, S_{H3}, and S_{H4} crystals synthesized with the use of mesoporegene PEG, which is further confirmed by N_2 adsorption/desorption measurement.

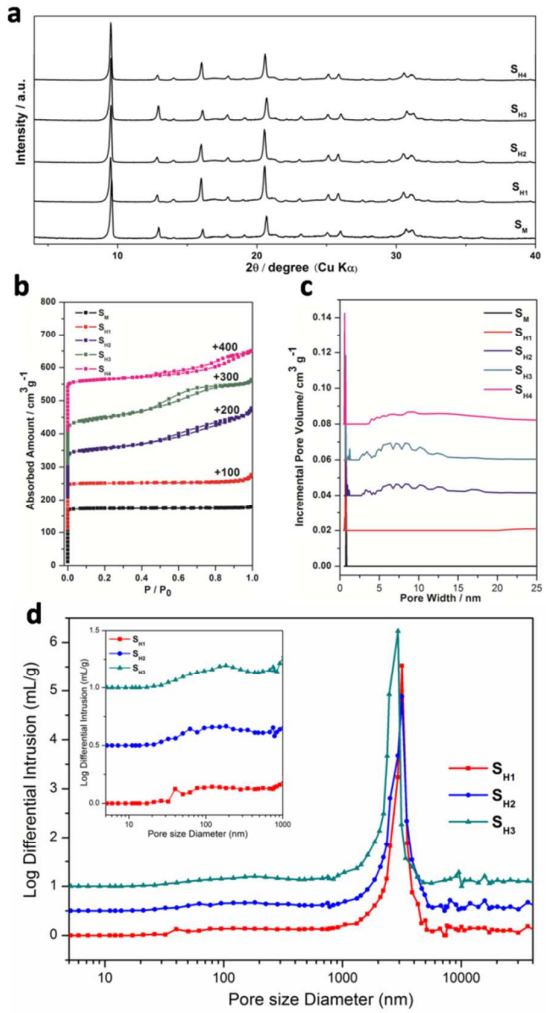

Figure 1. (a) XRD patterns, (b) N_2 adsorption/desorption isotherms, (c) DFT pore size distribution curves of conventional microporous SAPO-34 (S_M) and hierarchically porous SAPO-34 (S_{H1}, S_{H2}, S_{H3}, and S_{H4}) and (d) pore size distribution curves of hierarchically porous SAPO-34 (S_{H1}, S_{H2}, and S_{H3}) determined by mercury intrusion porosimetry.

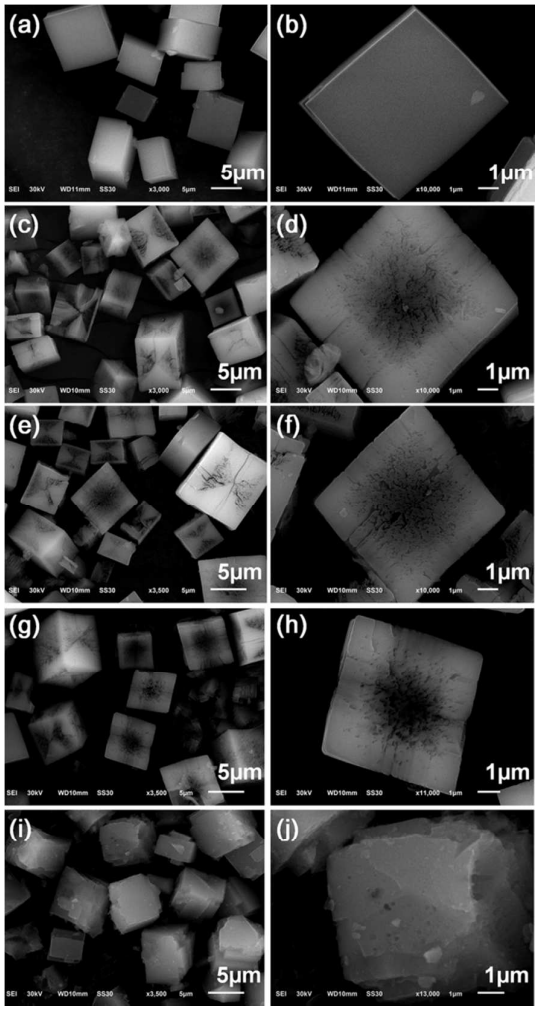

Figure 2. SEM images of conventional microporous SAPO-34 (S_M) (a, b) and hierarchically porous SAPO-34 (S_{H1} (c, d), S_{H2} (e, f), S_{H3} (g, h) and S_{H4} (i, j)).

Figure 1b shows the N_2 adsorption/desorption isotherms of the hierarchically porous SAPO-34 samples and the conventional counterpart. Samples S_M and S_{H1} display the characteristics Type I isotherms. Samples S_{H2}, S_{H3}, and S_{H4} exhibit the type-IV isotherms with the hysteresis loops in the region $0.4<P/P_o<0.9$, indicating the existence of mesopores.[41] In contrast to the conventional microporous SAPO-34 (S_M), the uptakes near saturation pressure in the isotherms of the SAPO-34 samples (S_{H1} , S_{H2} and S_{H3}) are observed, indicating that macropores exist in the hierarchically structured SAPO-34 samples. DFT pore size distribution curves also prove the existence of mesopores (3-15 nm) in the hierarchically porous SAPO-34 samples S_{H2}, S_{H3} and S_{H4}. Notably, the hierarchical sample S_{H3} displays significantly increased external surface (193 m^2/g) and mesopore volume (0.31 cm^3/g) as compared with the conventional microporous SAPO-34 due to the Al-rich and PEG 2000 introduced into the crystals. The detailed surface area and pore volume data are summarized in Table 1. Figure 1d shows the macropore size distributions of hierarchically porous SAPO-34 samples determined by mercury intrusion porosimetry. In accordance with the SEM and TEM

observations, there are two different sizes of macropore existed in the hierarchical SAPO-34 samples, that is, micrometer-sized macroholes (ca. 2 μm) corresponding to the central macropore of crystal and nanometer-sized macrochannels (ca. 100 nm) corresponding to the intracrystalline macrochannels.

Inductively coupled plasma (ICP) analyses show that the hierarchically porous SAPO-34 samples S_{H1} , S_{H2} and S_{H3} possess more aluminum and less phosphorus compared to the conventional microporous SAPO-34 sample and the content of aluminum is more than the sum of silicon and phosphorus. The hierarchically porous SAPO-34 sample S_{H4} synthesized with normal Al content using the PEG 2000 polymer has a similar composition to the conventional SAPO-34 sample S_M. Meanwhile, according to TG analyses, the hierarchically porous SAPO-34 samples S_{H2}, S_{H3} and S_{H4} display more weight lose, indicating that PEG 2000 are introduced into the hierarchically porous SAPO-34 crystals (Figure S1, ESI†). NH_3-TPD analyses reveal that the hierarchically porous SAPO-34 samples have lower acidic strength and concentration in strong acid sites compared to the conventional microporous SAPO-34 sample (Figure 4).

Table 1. Compositions and textural properties of conventional microporous SAPO-34 (S_M) and hierarchically porous SAPO-34 samples (S_{H1}, S_{H2}, S_{H3} and S_{H4}).

Sample No.	Molar Composition[a]	TG(wt%)[b]	S_{BET} (m^2/g)[c]	S_{micro} (m^2/g)[d]	S_{ext} (m^2/g)[d]	V_{micro} (cm^3/g)[d]	V_{meso} (cm^3/g)[e]
S_M	$Al_{0.46}P_{0.45}Si_{0.09}O_2$	16.6	546	533	13	0.26	0.01
S_{H1}	$Al_{0.52}P_{0.39}Si_{0.09}O_2$	17.6	491	474	17	0.23	0.05
S_{H2}	$Al_{0.52}P_{0.39}Si_{0.09}O_2$	24.3	530	397	133	0.19	0.28
S_{H3}	$Al_{0.53}P_{0.39}Si_{0.08}O_2$	26.9	513	320	193	0.15	0.31
S_{H4}	$Al_{0.48}P_{0.42}Si_{0.10}O_2$	19.3	541	451	90	0.21	0.17

[a] Measured by inductively coupled plasma (ICP); [b] weight loss of templates (%) measured by TG (Fig. S1, ESI†); [c] S_{BET}(total surface area) calculated by applying the BET equation using the linear part ($0.05<P/P_o<0.30$) of the adsorption isotherm; [d] S_{micro} (micropore area), S_{ext} (external surface area) and V_{micro} (micropore volume) calculated using the t-plot method; [e] V_{meso} (mesopore volume) calculated using the BJH method (from desorption).

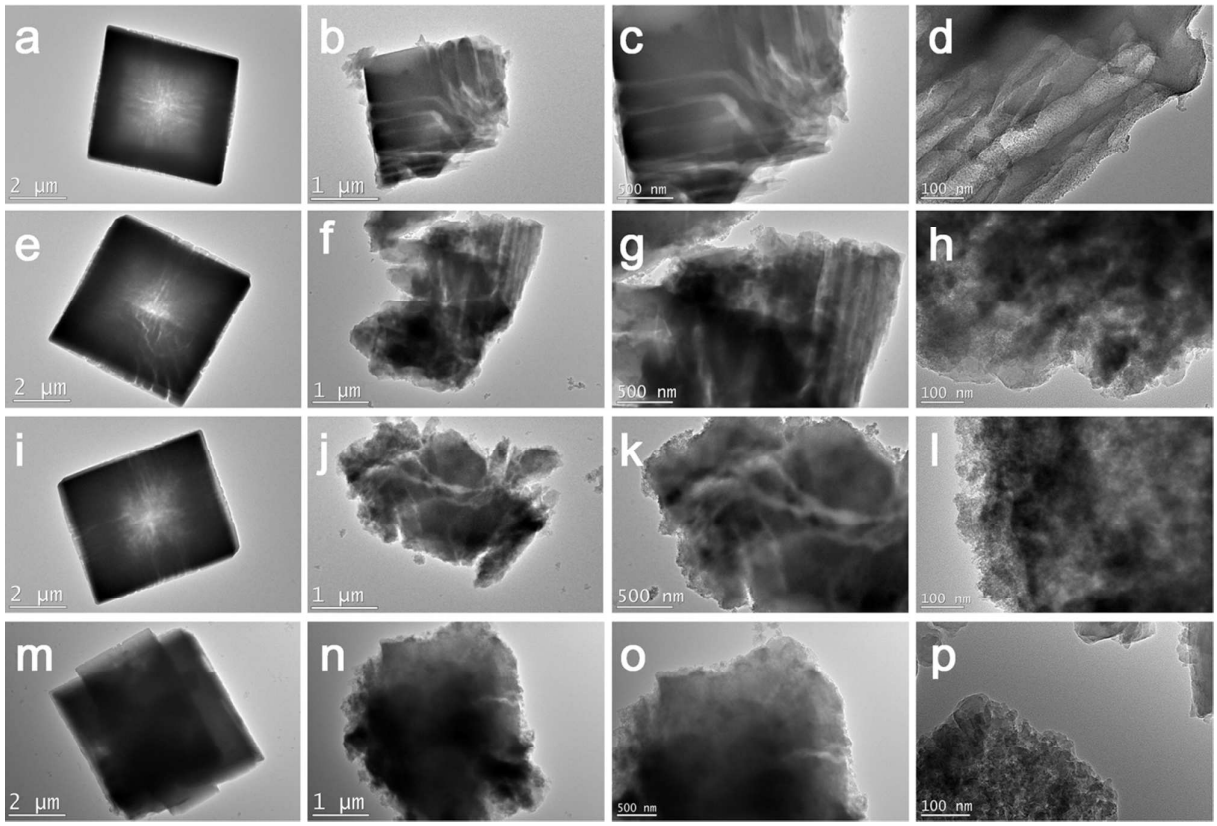

Figure 3. TEM images of hierarchically porous SAPO-34 crystals S_{H1} (a-d), S_{H2} (e-h), S_{H3} (i-l) and S_{H4} (m-p). Figures b-d, f-h, j-l, and n-p show the broken crystals by grinding S_{H1} , S_{H2}, S_{H3} and S_{H4} samples.

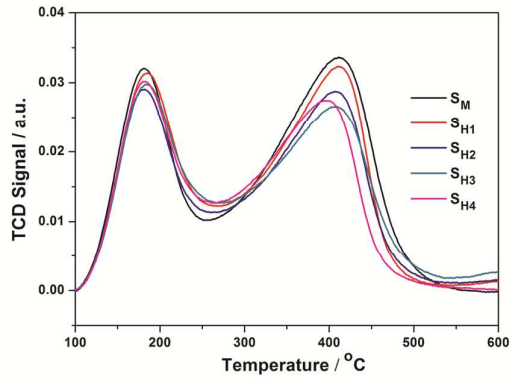

Figure 4. The NH_3-TPD curves of conventional microporous SAPO-34 (S_M) and hierarchically porous SAPO-34 (S_{H1}, S_{H2}, S_{H3}, and S_{H4}) catalysts.

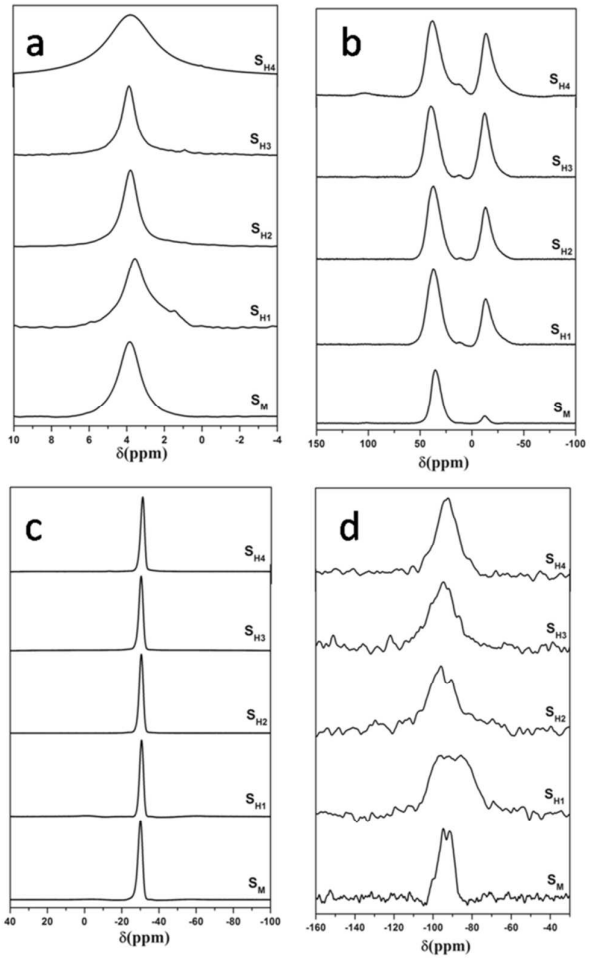

Figure 5. (a) ^{1}H, (b) ^{27}Al, (c) ^{31}P and (d) ^{29}Si MAS NMR spectra of conventional microporous SAPO-34 (S_M) and hierarchically porous SAPO-34 (S_{H1}, S_{H2}, S_{H3}, and S_{H4}) catalysts.

The solid-state ^{1}H, ^{27}Al, ^{31}P, and ^{29}Si MAS NMR spectra of the calcined SAPO-34 samples are shown in Figure 5. Compared to the conventional microporous SAPO-34, the hierarchically porous SAPO-34 crystals show more pentacoordinated and octahedral aluminum atoms as well as more coordination states of silicon atoms.[42, 43]

The proposed process forming the hollow tri-level hierarchical SAPO-34 zeolite with intracrystalline micro-meso-macropore structure is illustrated in Scheme 1. At the beginning, PEG attracts the zeolite precursors and directs them onto the surface of PEG micelles. In the process of crystallization, the PEG micelles are embedded into the zeolite crystal directing the mesoporous structure. Meanwhile, the superfluous aluminium in the SAPO-34 zeolite framework produces more defects and terminal groups leading to the formation of macroporores. The central parts of the hierarchical crystals are more easily etched during the process of crystallization, because of the intergrowth structure as indicating by SEM images, which leads to the formation of hollow morphology as observed in the previous work.[44]

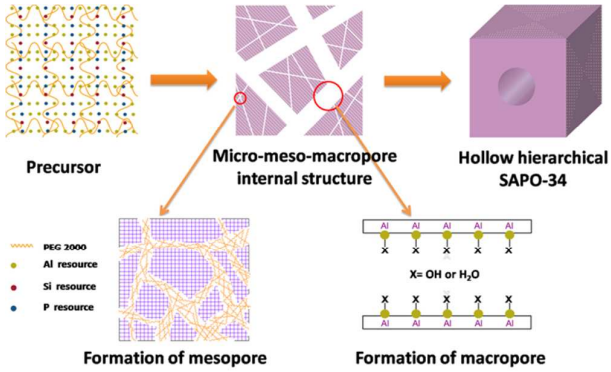

Scheme 1. The proposed process forming the hollow SAPO-34 zeolite with tri-level hierarchically intracrystalline micro-meso-macropore structure

Catalytic tests of methanol conversion were performed in a fixed bed reactor at 723 K over the hierarchical and conventional SAPO-34 catalysts. The conversions versus time-on-stream (TOS) and selectivities of products over the SAPO-34 catalysts are shown in Figures 6, S2–S8, and the detailed MTO results are summerized in Table S1. Compared to the conventional microporous SAPO-34 catalyst, the hierarchically porous SAPO-34 catalysts exhibit remarkably prolonged catalyst lifetimes. Notably, the lifetime of sample S_{H3} with tri-level hierarchically porous structure SAPO-34 reaches up to 386 min, which is about six-times higher than the lifetime of the microporous SAPO-34 S_M (66 min). In addition, the lifetime of tri-level hierarchical SAPO-34 S_{H3} is also much higher than that of the bi-level hierarchical SAPO-34 S_{H1} with micro-macroporosity (186 min) and SAPO-34 S_{H4} with micro-mesoporosity (226 min). Meanwhile, the selectivity of ethylene and propylene of the tri-level hierarchically porous SAPO-34 catalyst (84.2%) has improved nearly 5% compared to the conventional one (79.8%), and higher than that of the bi-level hierarchical SAPO-34 S_{H1} with micro-macroporosity (82.9%) and SAPO-34 S_{H4} with micro-mesoporosity (83.1%). Particularly, the hierarchical SAPO-34 catalysts show higher ethylene selectivity than the conventional one, which can be attributed to their decreased acidity.[32, 45] Meanwhile, the intracrystalline micro-meso-macropore structure in the hierarchically porous SAPO-34 catalysts can greatly enhance the transfer of the products from the narrow pore to outside space and reduce the coke formation and thus prolong the

lifetimes and improve the product selectivity. Provious studies has showed that hierarchical porosity can greatly improve the catalytic activity and selectivity due to the enhanced diffusion efficiency.[24, 46]

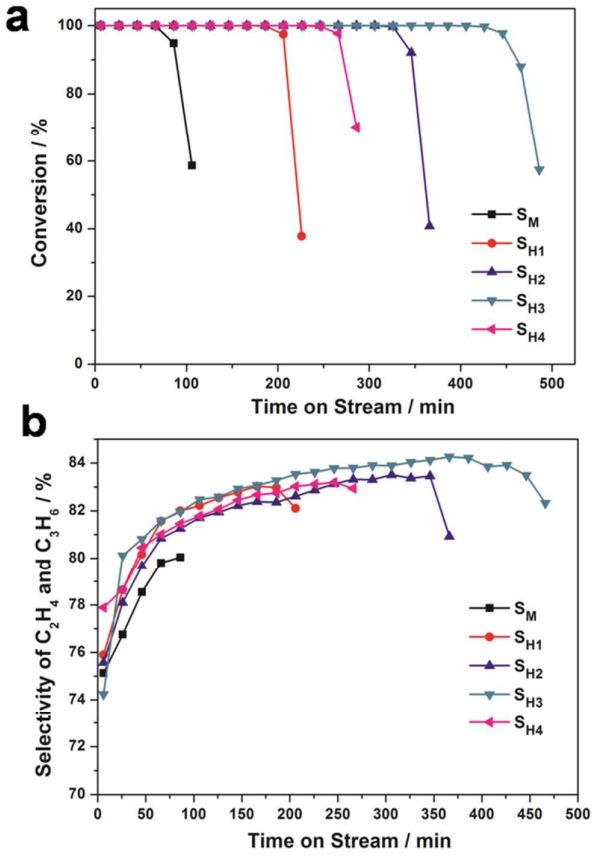

Figure 6. (a) Methanol conversion variation with time-on-stream and (b) Selectivity of C_2H_4 and C_3H_6 variation with time-on-stream over conventional microporous SAPO-34 (S_M) and hierarchically porous SAPO-34 (S_{H1}, S_{H2}, S_{H3}, and S_{H4}) catalysts in MTO reaction. Experimental conditions: WHSV = 4 h^{-1}, T = 723 K, catalyst weight = 300 mg.

In addition, the hierarchical pores can also provide more spaces to accommodate larger coke species such as phenanthrenes and pyrenes in comparison with the conventional micropore (Figure 7). The smaller coke species such as benzenes and naphthalenes can easily escape through the hierarchically structured SAPO-34 that slows down the formation of larger organic species, and thus prolong the catalytic lifetime. Furthermore, the decreased acidic strength and concentration of hierarchically porous SAPO-34 catalysts can also retard the coke formation and thus prolong the catalytic lifetime.[47] As shown in Figure S9, the hydrogen transfer indexs (HTI, C_3H_8/C_3H_6) over hierarchically porous SAPO-34 catalysts are greatly suppressed compared to the conventional catalyst. The coking rates over hierarchically porous SAPO-34 catalysts are much lower than the conventional catalyst, especially, sample S_{H3} with tri-level porosity possesses the lowest coking rate of 0.142 mg/min that is just one third of the conventional sample S_M (Table S2, ESI†).

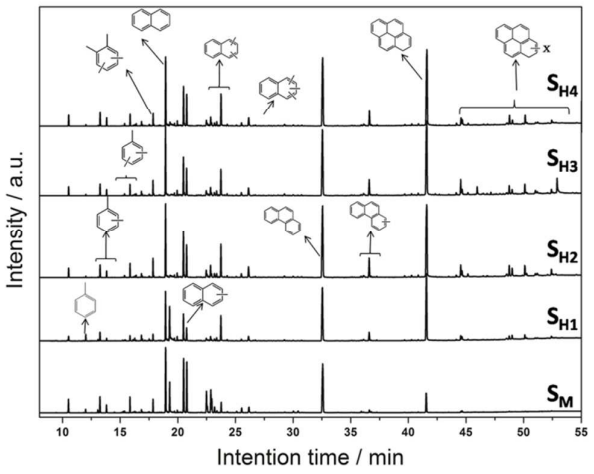

Figure 7. GC-MS chromatograms of occluded organic species retained in the SAPO-34 catalysts after methanol conversion at 723K. The structures annotated onto the chromatograms are peak identifications in comparison with the mass spectra to those in the NIST database.

4 Conclusions

In summary, the tri-level hierarchically porous SAPO-34 zeolite has been successfully synthesized using an Al-rich method coupled with the use of polymer under hydrothermal conditions. The as-prepared hierarchically porous SAPO-34 crystals possess the hollow cubic-like morphology with intracrystalline micro-meso-macropore structure. Thanks to the enhanced mass transport within the hierarchical porous system and decreased acidity, the tri-level hierarchical SAPO-34 catalyst exhibits superior MTO performance with about six-times prolonged catalytic lifetime and nearly 5% improvement of selectivity for light olefin (C_2H_4+C_3H_6) compared to the conventional microporous SAPO-34 catalyst. This work demonstrates a novel and simple synthetic route to prepare tri-level hierarchical zeolites with intracrystalline micro-meso-macroporosity showing superior catalytic activity, which will open new perspective for the application of tri-level hierarchically porous zeolites with unique textural properties.

Acknowledgements

We thank the State Basic Research Project of China (Grant No. 2011CB808703) and National Natural Science Foundation of China (Grant Nos: 91122029 and 21320102001) for supporting this work.

Notes and references

1 M. Moliner, C. Martinez and A. Corma, *Angew. Chem. Int. Ed.* 2015**, 54**, 3560-3579.
2 Y. Li and J. Yu, *Chem. Rev.* 2014**, 114**, 7268-7316.
3 J. Li, A. Corma and J. Yu, *Chem. Soc. Rev.* 2015, DOI: 10.1039/C5CS00023H.
4 A. Corma, *Chem. Rev.* 1997**, 97**, 2373-2420.
5 A. Corma, *J. Catal.* 2003**, 216**, 298-312.

6 J. Zhou, Z. Liu, Y. Wang, H. Gao, L. Li, W. Yang, Z. Xie and Y. Tang, *RSC Advances* 2014**, 4**, 43752-43755.
7 D. P. Serrano, J. M. Escola and P. Pizarro, *Chem. Soc. Rev.* 2013**, 42**, 4004-4035.
8 N. D. Petkovich and A. Stein, *Chem. Soc. Rev.* 2013**, 42**, 3721-3739.
9 J. G.-M. K. Li, Mesoporous Zeolites, Wiley VCH, 2014.
10 L.-H. Chen, X.-Y. Li, J. C. Rooke, Y.-H. Zhang, X.-Y. Yang, Y. Tang, F.-S. Xiao and B.-L. Su, *J. Mater. Chem.* 2012**, 22**, 17381-17403.
11 Z.-Y. Yuan and B.-L. Su, *J. Mater. Chem.* 2006**, 16**, 663-677.
12 M. Ojeda, A. Grau-Atienza, R. Campos, A. A. Romero, E. Serrano, J. Maria Marinas, J. García Martínez and R. Luque, *ChemSusChem* 2015**, 8**, 1328-1333.
13 M. Choi, K. Na, J. Kim, Y. Sakamoto, T. Osamu and R. Ryoo, *Nature* 2009**, 461**, 246.
14 D. Xu, Y. Ma, Z. Jing, L. Han, B. Singh, J. Feng, X. Shen, F. Cao, P. Oleynikov, H. Sun, O. Terasaki and S. Che, *Nat. Commun* 2014**, 5**. DOI: 10.1038/ncomms5262
15 C. Jo, J. Jung, H. S. Shin, J. Kim and R. Ryoo, *Angew. Chem.* 2013**, 125**, 10198-10201.
16 J. Zhu, Y. Zhu, L. Zhu, M. Rigutto, A. van der Made, C. Yang, S. Pan, L. Wang, L. Zhu, Y. Jin, Q. Sun, Q. Wu, X. Meng, D. Zhang, Y. Han, J. Li, Y. Chu, A. Zheng, S. Qiu, X. Zheng and F.-S. Xiao, *J. Am. Chem. Soc.* 2014**, 136**, 2503-2510.
17 I. Schmidt, A. Boisen, E. Gustavsson, K. Ståhl, S. Pehrson, S. Dahl, A. Carlsson and C. J. H. Jacobsen, *Chem. Mater.* 2001**, 13**, 4416-4418.
18 R. J. White, A. Fischer, C. Goebel and A. Thomas, *J. Am. Chem. Soc.* 2014**, 136**, 2715-2718.
19 Z. Qin, L. Lakiss, J. P. Gilson, K. Thomas, J. M. Goupil, C. Fernandez and V. Valtchev, *Chem. Mater.* 2013**, 25**, 2759-2766.
20 X. Chen, T. Todorova, A. Vimont, V. Ruaux, Z. Qin, J.-P. Gilson and V. Valtchev, *Micropor. Mesopor. Mater.* 2014**, 200**, 334-342.
21 X.-Y. Yang, G. Tian, L.-H. Chen, Y. Li, J. C. Rooke, Y.-X. Wei, Z.-M. Liu, Z. Deng, G. Van Tendeloo and B.-L. Su, *Chem. Eur. J.* 2011**, 17**, 14987-14995.
22 L.-H. Chen, X.-Y. Li, G. Tian, Y. Li, J. C. Rooke, G.-S. Zhu, S.-L. Qiu, X.-Y. Yang and B.-L. Su, *Angew. Chem. int. ed.* 2011**, 50**, 11156-11161.
23 K. P. de Jong, J. Zečević, H. Friedrich, P. E. de Jongh, M. Bulut, S. van Donk, R. Kenmogne, A. Finiels, V. Hulea and F. Fajula, *Angew. Chem.* 2010**, 122**, 10272-10276.
24 B. Li, Z. Hu, B. Kong, J. Wang, W. Li, Z. Sun, X. Qian, Y. Yang, W. Shen, H. Xu and D. Zhao, *Chem. Sci.* 2014**, 5**, 1565-1573.
25 C. D. Chang, *Catal. Rev.* 1983**, 25**, 1-118.
26 C. D. Chang, *Catal. Rev.* 1984**, 26**, 323-345.
27 D. Chen, K. Moljord and A. Holmen, *Micropor. Mesopor. Mater.* 2012**, 164**, 239-250.
28 U. Olsbye, S. Svelle, M. Bjørgen, P. Beato, T. V. W. Janssens, F. Joensen, S. Bordiga and K. P. Lillerud, *Angew. Chem. int. ed.* 2012**, 51**, 5810-5831.
29 P. Tian, Y. X. Wei, M. Ye and Z. M. Liu, *Acs. Catal.* 2015**, 5**, 1922-1938.
30 Y. Li, M. Zhang, D. Wang, F. Wei and Y. Wang, *J. Catal.* 2014**, 311**, 281-287.
31 W. L. Dai, C. M. Wang, M. Dyballa, G. J. Wu, N. J. Guan, L. D. Li, Z. K. Xie and M. Hunger, *Acs. Catal.* 2015**, 5**, 317-326.
32 Q. Sun, N. Wang, D. Xi, M. Yang and J. Yu, *Chem. Commun.* 2014**, 50**, 6502-6505.
33 C. Wang, M. Yang, P. Tian, S. Xu, Y. Yang, D. Wang, Y. Yuan and Z. Liu, *J. Mater. Chem. A* 2015**, 3**, 5608-5616.
34 D. Xi, Q. Sun, J. Xu, M. Cho, H. S. Cho, S. Asahina, Y. Li, F. Deng, O. Terasaki and J. Yu, *J. Mater. Chem. A* 2014**, 2**, 17994-18004.
35 Y. Li, Y. Huang, J. Guo, M. Zhang, D. Wang, F. Wei and Y. Wang, *Catal. Today* 2014**, 233**, 2-7.
36 H. Yang, Z. Liu, H. Gao and Z. Xie, *J. Mater. Chem.* 2010**, 20**, 3227-3231.
37 Y. Cui, Q. Zhang, J. He, Y. Wang and F. Wei, *Particuology* 2013**, 11**, 468-474.
38 J. Tan, Z. Liu, X. Bao, X. Liu, X. Han, C. He and R. Zhai, *Micropor. Mesopor. Mater.* 2002**, 53**, 97-108.
39 G. Sastre, D. W. Lewis and C. R. A. Catlow, *J. Phys. Chem. B* 1997**, 101**, 5249-5262.
40 Y. Liu, W. Qu, W. Chang, S. Pan, Z. Tian, X. Meng, M. Rigutto, A. Made, L. Zhao, X. Zheng and F.-S. Xiao, *J. Colloid Interface Sci.* 2014**, 418**, 193-199.
41 M. Choi, R. Srivastava and R. Ryoo, *Chem. Commun.* 2006, 4380-4382.
42 S. Ashtekar, S. V. V. Chilukuri and D. K. Chakrabarty, *J. Phys. Chem.* 1994**, 98**, 4878-4883.
43 W. Shen, X. Li, Y. Wei, P. Tian, F. Deng, X. Han and X. Bao, *Micropor. Mesopor. Mater.* 2012**, 158**, 19-25.
44 J. Gong, F. Tong, X. Ji, C. Zeng, C. Wang, Y. Lv and L. Zhang, *Cryst. Growth Des.* 2014**, 14**, 3857-3863.
45 M. Kang and T. Inui, *Catal. Lett.* 1998**, 53**, 171-176.
46 J. Kim, M. Choi and R. Ryoo, *J. Catal.* 2010**, 269**, 219-228.
47 Q. Sun, Y. Ma, N. Wang, X. Li, D. Xi, J. Xu, F. Deng, K. B. Yoon, P. Oleynikov, O. Terasaki and J. Yu, *J. Mater. Chem. A* 2014, **2**, 17828-17839.

Table of contents

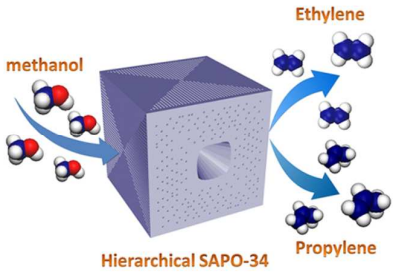

Tri-level hierarchically porous SAPO-34 zeolite with intracrystalline micro-meso-macropore structure has been synthesized exhibiting remarkably enhanced performance in methanol-to-olefin reaction.